Electronic Supporting Information

Catalysis of Water Oxidation in Acetonitrile by Iridium Oxide Nanoparticles

Jonnathan C. Hidalgo-Acosta,[a] Manuel A. Méndez,[a] Micheál D. Scanlon,[a] Heron Vrubel,[a]

Veronique Amstutz,[a] Wojciech Adamiak[b], Marcin Opallo[b] and Hubert H. Girault[a]*

[a]Laboratoire d'Electrochimie Physique et Analytique, Ecole Polytechnique Fédérale de Lausanne, CH-1015 Lausanne, Switzerland.
*Fax : (+) 41 21 6933667, Email : Hubert.Girault@epfl.ch

[b]Institute of Physical Chemistry, Polish Academy of Sciences, ul. Kasprazaka 44/52,01-224 Warszawa, Poland

Table of Contents

S1: Experimental Methods

S1.1: Chemicals.

All chemicals were used as received without further purification. Ruthenium (III) chloride hydrate ($RuCl_3 \cdot x H_2O$, 99.98%), potassium hexachloroiridate (K_2IrCl_6, 99.99%), tri-sodium citrate dihydrate (≥99.0) and sodium bicarbonate ($NaHCO_3$, ≥99.5) were purchased from Aldrich. Tetrabutylammonium hexafluorophosphate ($TBAPF_6$, ≥99.0%), sodium hexafluorosilicate (Na_2SiF_6, 97%) and activated manganese oxide (MnO_2, technical grade) were ordered from Fluka, 2,2'-Bipyridine (>99%) was purchased from Acros, while potassium hexafluorophosphate (KPF_6, 99.5%) was received from Strem chemicals. Sulphuric acid (H_2SO_4 (95-98%) and perchloric acid ($HClO_4$ (70%) were purchased from Aldrich. All aqueous solutions were prepared with ultrapure water (Millipore Milli-Q, specific resistivity 18.2 MΩ•cm). The organic solvents dimethyl sulfoxide (DMSO, ≥99.9%), toluene (>99.5%), acetone (>99.5%), diethylether (>99.8%) and ethanol (>99.8%) were purchased from Sigma. Acetonitrile (ACN, extra dry over molecular sieves, 99.9%) was ordered from Acros. Pure oxygen cylinders were purchased from Carbagas.

S1.2: Synthetic Protocols.

S1.2.1: Synthesis of Ru(bpy)$_3$Cl$_2$·6H$_2$O.

Ru(bpy)$_3$Cl$_2$ was prepared using Ru(DMSO)$_4$Cl$_2$ as the starting material. The latter complex was prepared as reported by Evans *et al.*[1] Briefly, 3.82 mmol of RuC1$_3$.xH$_2$O was

dissolved in 5 ml of DMSO and refluxed for 5 min. The mixture turned a brown-orange colour when the reaction was complete. The solution volume was subsequently reduced to 0.5-1.0 mL by passing a gentle stream of nitrogen gas over the gently heated liquid. The addition of acetone (20 mL) produced a yellow precipitate that was separated by filtration. This yellow solid was washed with acetone and vacuum dried.

In a typical synthesis, 1.34 mmol of $Ru(DMSO)_4Cl_2$ was placed in a 100 mL round-bottom flask along with 4.68 mmol of 2,2'-bipyridine and 50 mL of ethanol. The mixture was refluxed with continuous stirring until the solution turned red-orange. This colour change typically took no more than 1 hour. The obtained product was dried and the solid washed with toluene in order to remove excess ligand. The dry solid was dissolved in water and slowly dropped into acetone. Finally, the precipitate was filtered, washed with acetone and dried under vacuum.

S1.2.2: Synthesis of $Ru(bpy)_3(PF_6)_2$.

The synthesis was carried out as described by Ji *et al.*[2] Briefly, 1.16 mmol of $Ru(bpy)_3Cl_2·6H_2O$ was dissolved in 20 mL of water and added drop wise into an equal volume of a warm stirring solution containing 5.81 mmol of aqueous KPF_6. The obtained orange product was kept under stirring conditions for two hours, filtered, washed with cold water and dried under vacuum. The obtained powder was dissolved in the minimum amount of acetone and precipitated by the addition of diethylether. The microcrystalline product was filtered, washed with ether and dried under vacuum overnight. The yield was 92%.

S1.2.3: Synthesis of $Ru(bpy)_3(PF_6)_3$.

The synthesis was adapted from the procedures reported by Biner et $al.$[3] and DeSimone et $al.$[4] Briefly, 0.303 mmol of Ru(bpy)$_3$Cl$_2$·6H$_2$O was dissolved under stirring in 6 mL of 7 M H$_2$SO$_4$. After that, the solution was cooled in an ice/water bath. The addition of 36 mg of MnO$_2$ immediately produced a colour change in the solution from orange to green. After 1 hour, the excess MnO$_2$ was separated by filtration and the liquid mixed slowly with 4.4 mL of 0.42 M aqueous KPF$_6$. The final step produced a green precipitate, which was filtered under vacuum and washed with a small amount of pure cold water. No decomposition of the product was observed under these conditions. The final solid was dried under vacuum for at least 4 hours. The obtained product obtained was stable for several months once stored in a refrigerator.

S1.2.4: Synthesis of colloidal iridium oxide nanoparticles (IrO$_2$ NPs).

The synthesis was performed as detailed by Mallouk and co-workers.[5, 6] 0.0300 g of K$_2$IrCl$_6$ (6.20x10^{-5} moles) and 0.0547 g of tri-sodium citrate dihydrate (1.86x10^{-4} moles) were weighed out, placed in a 50 mL volumetric flask and filled up to the mark with de-ionized water. The pH of this solution was adjusted with 0.25 M NaOH to approximately 7.5. The brown solution was then transferred to a 100 mL round bottomed flask with a reflux condenser attached and heated at 95°C in an oil bath. After 30 min. the round-bottomed flask was removed from the oil-bath and the solution cooled to room temperature. The pH of this solution was precisely adjusted to 7.5 with 0.25 M NaOH. The addition of NaOH solution at room temperature, followed by heating at 95 °C for 30 min. was repeated until the pH had stabilized at 7.5. The solution was heated again at 95 °C for 2 hours with oxygen bubbling through the solution. The colloidal solution was cooled to room temperature. Once the solution was cooled the IrO$_2$ solution was dialyzed in deionized water using Spectra/Pore 7 membranes with molecular weight

cut-offs (MWCO) of 1 kDa. The dialysis was performed over a 24-hour period and the deionized water solution changed 4 times. The final solution was diluted to a total volume of 100 mL to render a 0.62 mM solution of IrO_2.

S1.3: ^{1}H NMR spectroscopy.

^{1}H NMR analysis was performed in an NMR tube on a Bruker Biospin Avance-400 spectrometer. Chemical shifts were expressed in parts per million (ppm) relative to tetramethylsilane (TMS). The NMR spectra were acquired after the desired time for the reaction was reached. For these experiments, the water/ACN mixtures were prepared using D_2O and ACN-D3

S1.4: Gas chromatography.

The quantitative determination of the amounts of molecular oxygen (O_2) evolved from the samples was achieved by taking into account O_2 distributed both in the head space and in the solution. The number of moles of O_2 in the head space ($\%O_2$) was calculated from the percentage obtained according to the calibration curve (($\%O_2$), Figure S1, see below) as follows:

$$\eta_{O_{2(HS)}} = \left(\frac{\%O_2}{100 - \%O_2} \right) \left(\frac{P_{atm} \times V_{HS}}{R \times T} \right) \tag{S1}$$

where P_{atm} is the atmospheric pressure, V_{HS} the volume of the head space, T the room temperature and R the gas constant. Additionally, the number of moles of dissolved O_2 in solution ($\eta_{O_{2(Sol)}}$) was calculated using Henry's law as follows:

$$\eta_{O_{2(Sol)}} = V_{sol} \times P_{O_2} \times H$$

*

MERGEFORMAT (S1)

where P_{O2} is the partial pressure and H is Henry's constant. An approximate value of H was taken and assumed to be that of pure ACN (2.42×10^{-3} M·Pa^{-1}).[7] Assuming ideal gas behavior, the partial pressure of O_2 (P_{O_2}) can be expressed as:

$$P_{O_2} = \frac{\eta_{O_{2HS}} \times R \times T}{V_{HS}}$$

*

MERGEFORMAT (S2)

Finally, the total number of moles of O_2 evolved was calculated as the sum of $\eta_{O_{2(HS)}}$ and $\eta_{O_{2(Sol)}}$.
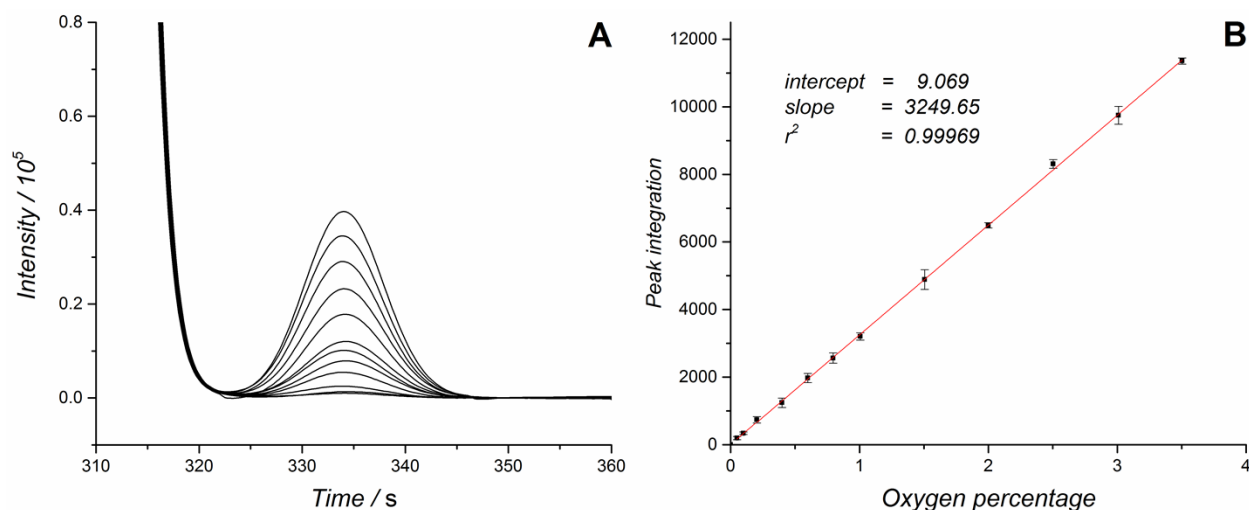
Figure S1. (A) Plot of GC data for gas samples with increasing concentrations of O_2 from bottom to top. **(B)** Calibration curve obtained by plotting the the area of the O_2 peak in the chromatogram *vs*. the fraction of O_2 in the head-space. Each point on the curve is the average of three measurements and the errors bars represent two times the standard deviation. Samples with differents amounts of O_2 were obtained by succesive dilution of an O_2 standard with N_2.

S1.5 Infra-red (IR) spectroscopy.

Water/ACN mixtures tested by IR spectroscopy were prepared by mixing ACN with water containing 20 % D_2O. The O-D and C≡N stretching bands for HDO and ACN in the mixtures at various water mole fractions (X_{H2O}) were measured at room temperature (25 °C) from 2000 to 3000 cm^{-1} on a Varian 800 FT-IR ATR Spectrometer.

S1.6: Bulk electrolysis.

The experimental details of how the electrochemical measurements, including bulk electrolysis, were performed in organic media are available in the Experimental section of the main text. The actual bulk electrolysis electrochemical cell is shown here.
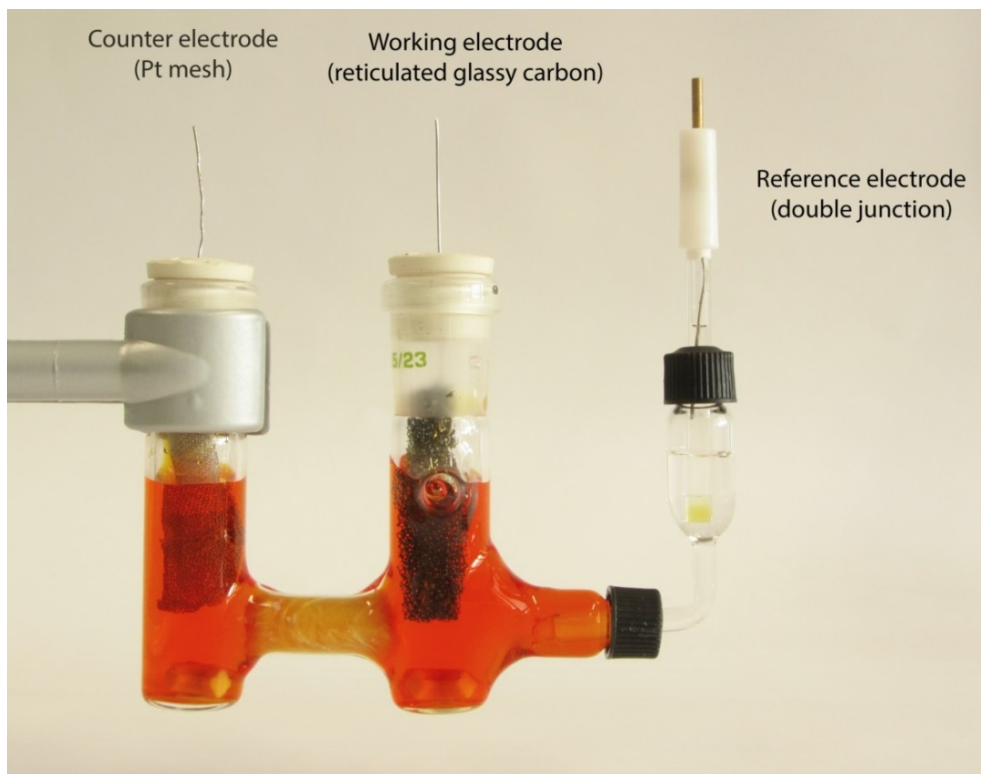
Figure S2. Cell used for bulk electrolysis experiments.

S1.7: Viscosity measurements.

Viscosity measurements were carried at room temperature (25°C) in a viscometer SV-A series, Stand Type A&D Company, limited.

S2: Characterization of Ru^{III}(bpy)$_3$(PF$_6$)$_3$ and its reduced form Ru^{II}(bpy)$_3$(PF$_6$)$_2$

S.2.1: Spectroscopic characterization.
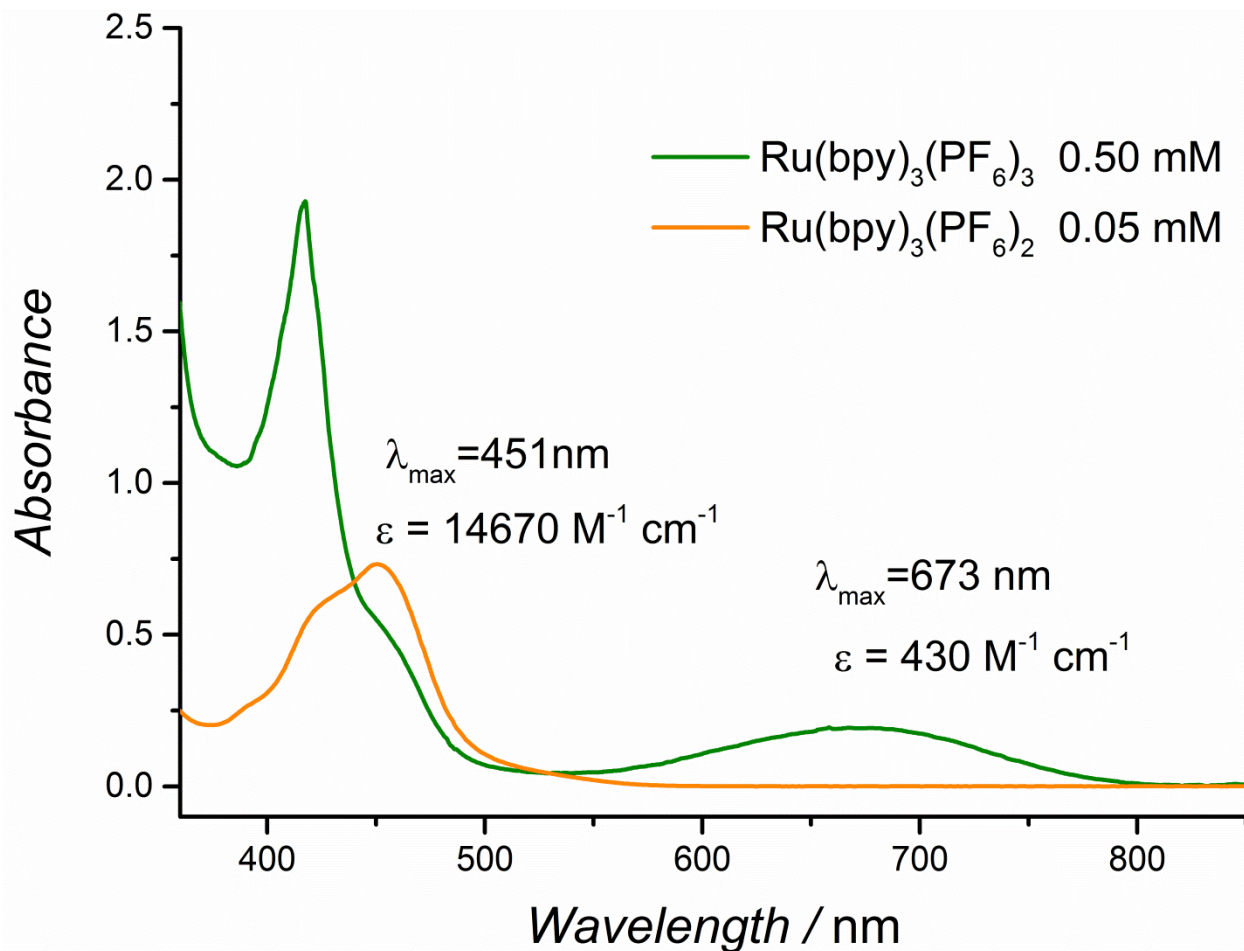
Figure S3. UV/vis absorbance spectra of 0.05 mM Ru (bpy)$_3$(PF$_6$)$_2$ and 0.50 mM Ru(bpy)$_3$(PF$_6$)$_3$ in dry ACN. At the concentrations used herein, it is more suitable to follow the kinetics of [Ru(bpy)$_3$]$^{3+}$ reduction as the disappearance of the band at 673 nm rather than the appearance of the MLCT band at 451 nm.

S2.2: Elemental analysis.

Table S1. Elemental analysis $Ru^{II}(bpy)_3(PF_6)_2$.

Element	% expected	% experimentally observed
C	41.9	41.5
H	2.8	3.0
N	9.8	9.6

Table S2. Elemental analysis $Ru(bpy)_3(PF_6)_3$

Element	% expected	% experimentally observed
C	35.9	35.6
H	2.4	2.0
N	8.4	8.1

S2.3: ^1H NMR spectroscopy.

The characteristic ^1H NMR spectrum associated with the pure $Ru^{II}(bpy)_3(PF_6)_2$ can be observed in the Figure S4. In the case of $Ru^{III}(bpy)_3(PF_6)_3$ a rather broad and poorly defined signal is obtained due to the paramagnetic properties of the metallic Ru center. Consequently, no information about the purity can be obtained.
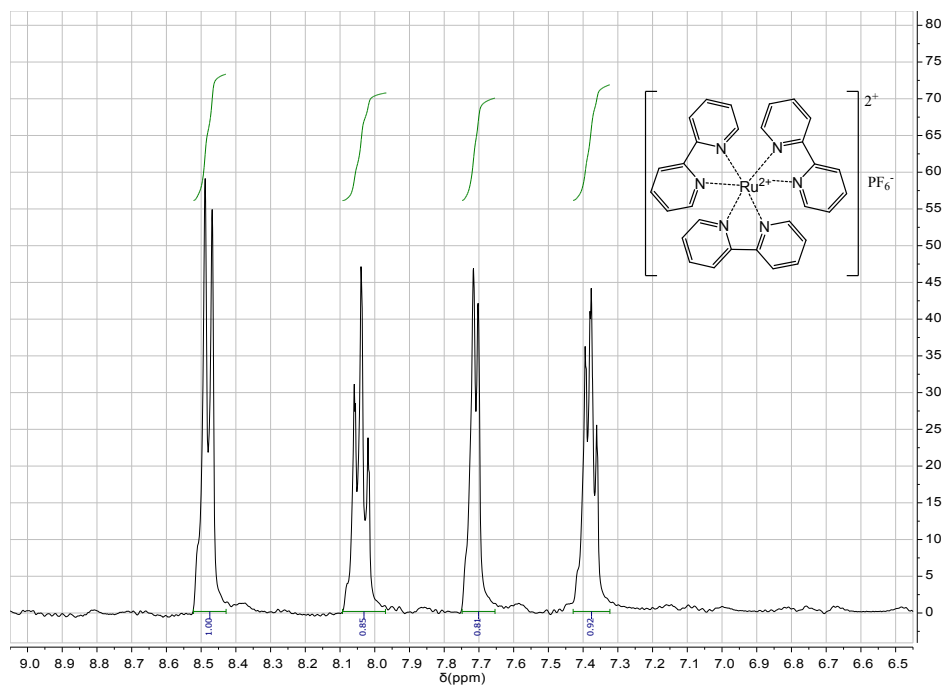
Figure S4. NMR spectrum for pure $Ru^{II}(bpy)_3(PF_6)_2$ in ACN-D3.

S2.4: Electrochemical characterization.

All electrochemical measurements in organic media were performed in a three-electrode configuration using a PGSTAT 30 potentiostat (Metrohm, CH). No iR compensation was applied to the cell. All voltammetry experiments were completed using organic media thoroughly de-gassed with nitrogen, under anaerobic conditions in a glovebox filled with nitrogen ($O_2 < 5$ ppm, $H_2O < 1$ ppm) and at an ambient temperature of 23 ± 2 °C.

Electrochemical characterization of the chemically synthesized hydrophobic electron acceptor $Ru^{III}(bpy)_3(PF_6)_3$ and its reduced form $Ru^{II}(bpy)_3(PF_6)_2$ was carried out in pure dry ACN containing 0.1 M tetrabutylammonium hexafluorophosphate (TBAPF$_6$) as supporting electrolyte. The three-electrode configuration employed a glassy carbon (GC, 0.071 cm²) disk working electrode, a platinum (Pt) wire counter electrode and a Ag/Ag$^+$ double junction organic

reference electrode (pictured in Figure S2, *vide supra*). The reference electrode was constructed from a Ag wire immersed in an ACN solution containing 0.1 M TBAPF$_6$ and separated from a compartment containing the same solution by a porous Vycor tip (BASI). The latter compartment was in turn separated from the main solution by a second Vycor tip. Prior to the experiments, the GC electrode was polished with 1.0 and 0.05 μm Al$_2$O$_3$ slurry to obtain a mirror surface followed by sonication in distilled water for 5 min. to remove debris and was thoroughly rinsed with Milli-Q ultrapure water. All voltammetric data is reported *versus* the ferrocene/ferrocenium cation (*vs.* Fc/Fc$^+$) redox couple. Calibration of the potential window was performed immediately after each measurement by injecting 1 mM Fc and recording cyclic voltammograms (CVs).
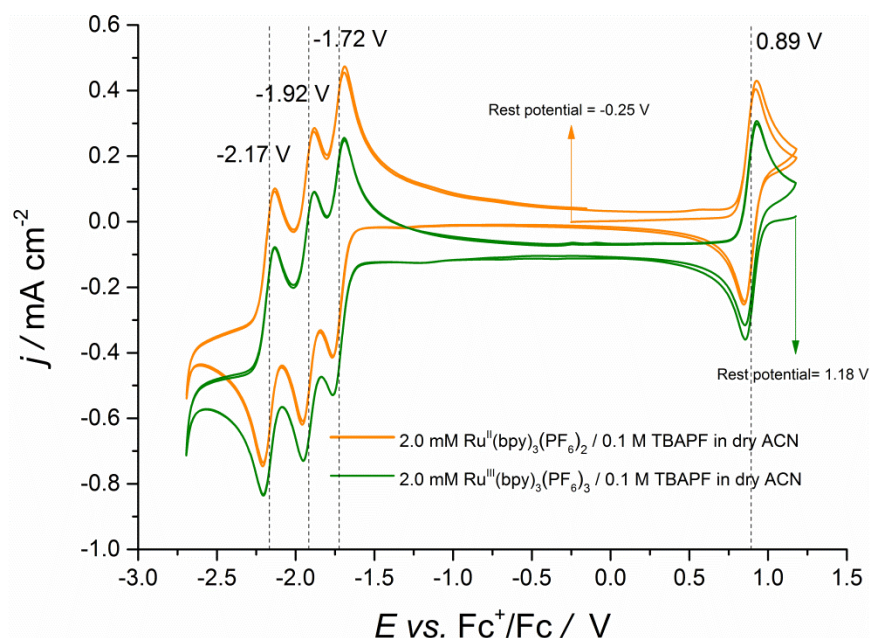
Figure S5. Cyclic voltammograms of 2 mM Ru(bpy)$_3$(PF$_6$)$_2$ and 2 mM Ru(bpy)$_3$(PF$_6$)$_3$ (containing 0.1 M tetrabutylammonium hexafluorophosphate (TBAPF$_6$) as supporting electrolyte) obtained with a glassy carbon electrode at a scan rate of 50 mVs^{-1}. The voltammetry was performed in dry ACN and under anaerobic conditions as described above.

S3: Characterization of colloidal IrO$_2$ NPs

S3.1: UV/vis spectroscopy.
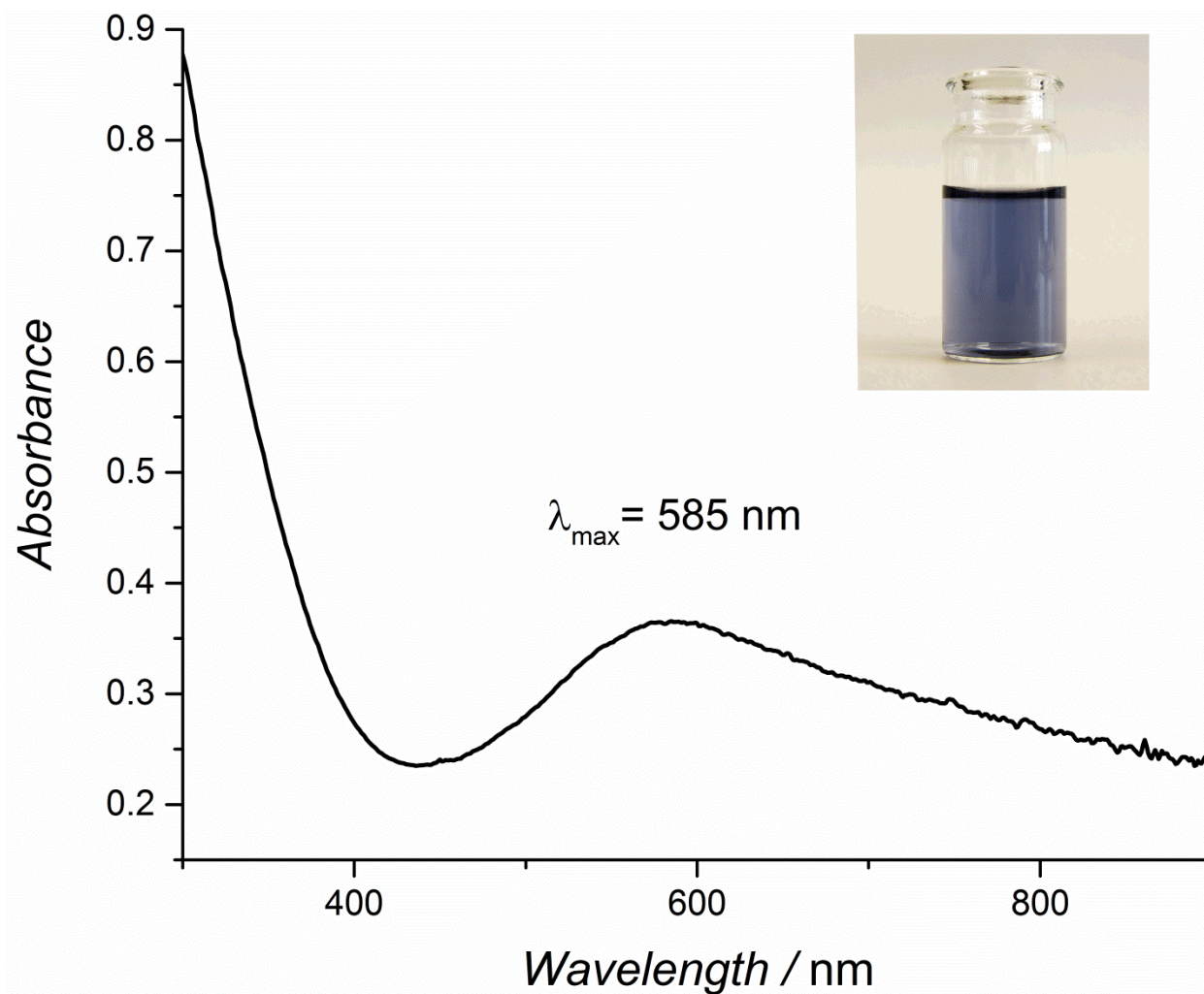
Figure S6. UV/vis absorbance spectra of IrO$_2$ NPs stabilized with citrate. A cell containing the blue colloid is shown in the inset. The spectrum exhibits an intense UV absorbance below 400 nm, and a broad band with maximum 585 nm that extends into the near-IR.

S3.2: Transmission electron microscopy (TEM).
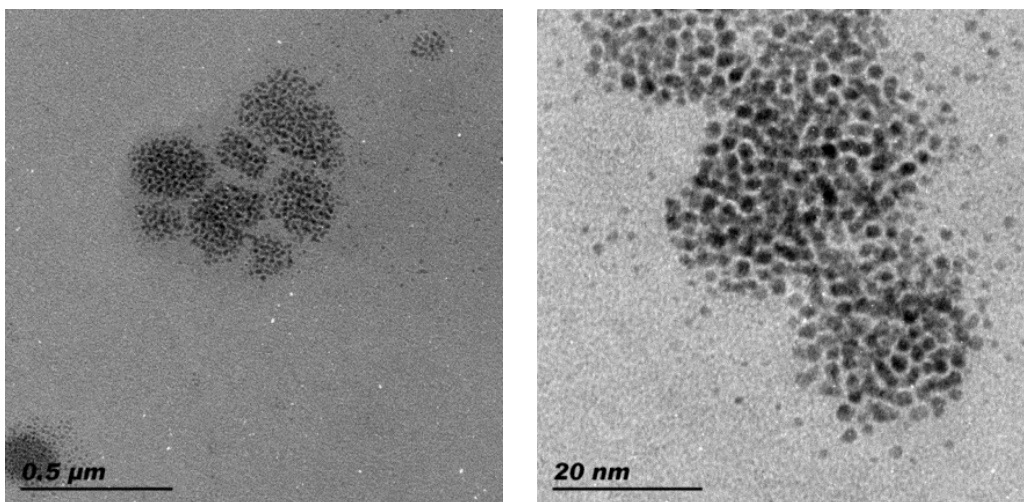
Figure S7. TEM images of citrate stabilized IrO_2 NPs at two different magnifications. The NPs are present as large agregates (>100 nm) that, upon closer inspection, are revealed to consist of clusters composed of much smaller particles (2 nm). The formation of large aggregates is presumably caused by the third carboxylate group of citrate, which is oriented away from the IrO_2 surface.[8]

S3.3: Control experiment: demonstrating the hydrophilic nature of the surface of IrO_2 NPs

In order to highlight the hydrophilicity of our as-prepared IrO_2 colloidal NPs, a simple experiment involving a biphasic system was devised. Figure S8 shows a biphasic system composed of a water-rich phase (on the bottom) and an ACN-rich phase (on top), prepared as detailed in the section *"Designing a model system for water oxidation in a non-aqueous environment"*. On injection of 100 μl of 6.2 mM IrO_2 NPs, followed by stirring and time to settle, the IrO_2 NPs preferentially occupy the bottom water-rich phase, as clearly indicated by the

blue colour, demonstrating the highly hydrophilic nature of the IrO_2 surface.
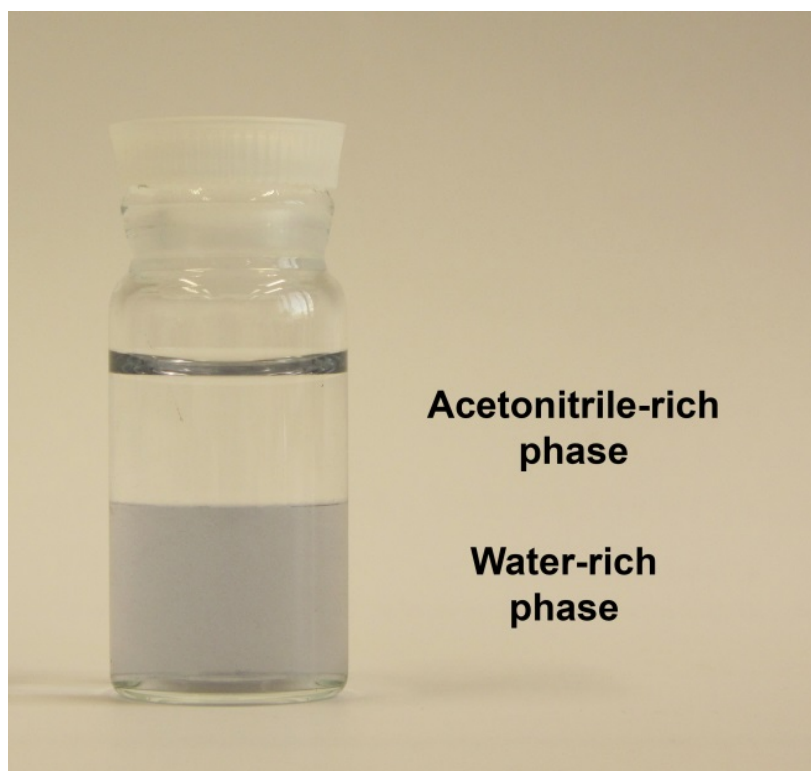
Figure S8. Biphasic system formed by a water-rich phase and an ACN-rich phase following injection of 100 μL of 6.2 mM IrO_2 NPs, stirring and allowing time to settle.

S4: Designing a model system for water oxidation in a non-aqueous environment

S4.1: Control experiment; monitoring the stability of Ru^{III}(bpy)$_3$(PF$_6$)$_3$ in ACN.
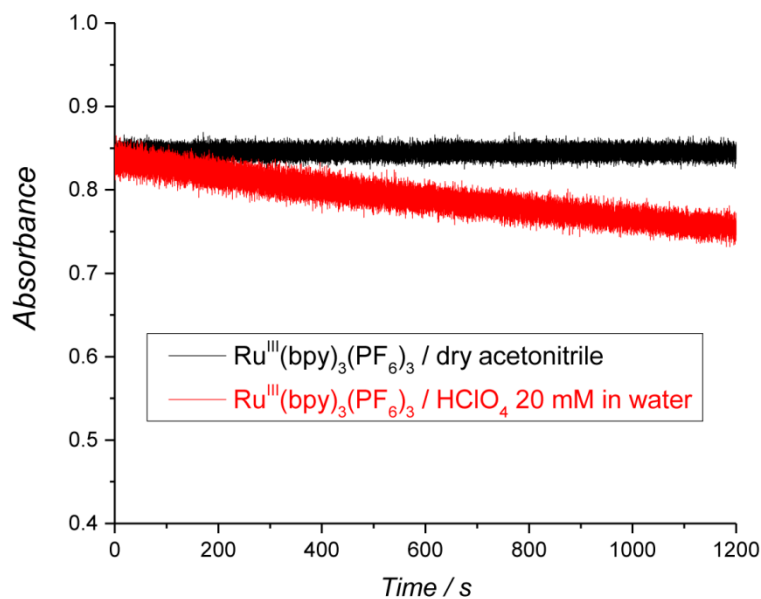
Figure S9. Real time absorbance measurements at 673 nm for 2 mM Ru(bpy)$_3$(PF$_6$)$_3$ dissolved in dry ACN and an aqueous solution of 20 mM HClO$_4$.

S5: Influence of "acidity regulators" and [IrO$_2$ NP] on the kinetics of the WOR

S.5.1: Validation of the "pre-mixing" and background subtraction protocols

Figure S10 shows typical UV/vis absorbance-time traces obtained at two different wavelengths, 673 nm (where [Ru^{III}(bpy)$_3$]$^{3+}$ absorbs) and 900 nm (the background absorption). It is noteworthy that with our experimental procedure, involving pre-mixing of water/ACN prior to injection into the pure dry ACN solvent, the absorbance peak spikes or instabilities that inevitably appear due to the turbulence of mixing, and associated with dramatic changes in the optical properties of the system, are restricted to the first second (clearly illustrated in Figure S10). This fact has been taken into account by elimination of the data within the first second after catalyst addition (see Figures 2 C & D in the main text) for kinetic analysis. The baseline correction procedure involving subtraction of the absorbance values of the background at 900 nm from the signal due to [Ru^{III}(bpy)$_3$]$^{3+}$ at 673 nm is also clearly authenticated in Figure S10.
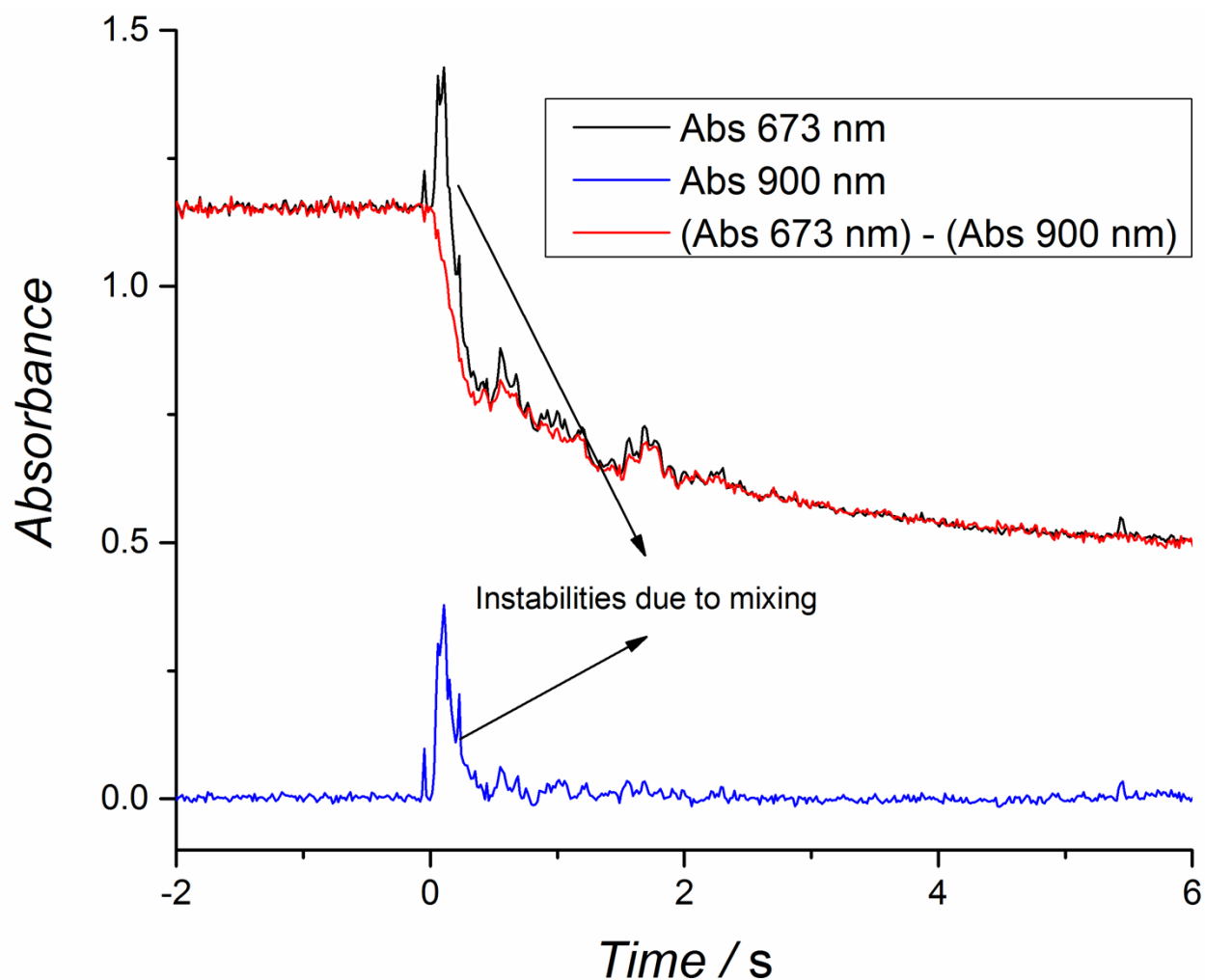
Figure S10. Baseline correction procedure. Real time absorbance measurements at 673 and 900 nm for $[Ru^{III}(bpy)_3]^{3+}$ solutions after the injection of a mixture containing water, ACN, $NaHCO_3/Na_2SiF_6$ buffer and IrO_2 NPs. The final content of water was 10 % (v/v).

S5.2: Control experiment; the necessity of an "acidity regulator" to obtain meaningful kinetics.

As highlighted in Figure S11, in the absence of buffer no linear correlation exists between ln[absorbance] and time in the crucial interval between 0 to 5 s for kinetics analysis. As

shown in Figure 2 in the main text, however, the presence of an acidity regulator eliminates such anomalies allowing highly accurate determination of kinetic rate contents in a water/ACN biphasic system.
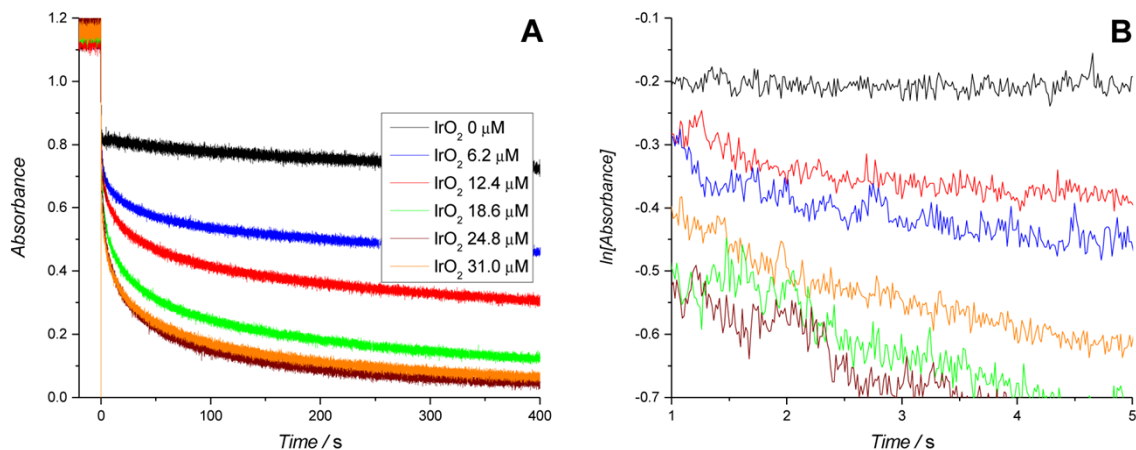
Figure S11. (A) Real time absorbance measurements for $[Ru^{III}(bpy)_3]^{3+}$ solutions after the addition of a mixture containing water, ACN and IrO_2 NPs in different concentrations. The absorbance was plotted as the difference between the values at 673 nm and 900nm. The final content of water was 10 % (v/v). **(B)** Plots of ln[Absorbance] *vs.* time derived from the data in (A).

S5.3: Influence of "acidity regulators" on the kinetics of $[Ru^{III}(bpy)_3^{3+}]$ reduction.

Herein, we describe in detail how each sample of varying $[IrO_2$ NP] in the presence of either a $HClO_4$ or $NaHCO_3/Na_2SiF_6$ "acidity regulator" was prepared for kinetics analysis. In a typical experiment 1.5 mL of 2.67 mM $Ru^{II}(bpy)_3(PF_6)_3$ dissolved in dry ACN was placed in a quartz cuvette. Next, 0.5 mL of a water/ACN mixture (0.4:1 v/v) was injected under vigorous

stirring and the absorbance values at 673 nm and 900 nm recorded as a function of time. The mixtures added were prepared as shown in the table S3.

Table S3. Summary of the mixtures containing IrO_2 NPs, water and ACN used in the experiments to study the influence of the "acidity regulator" and the concentration of the IrO_2 NP catalyst on the kinetics responses. The "acidity regulator" stock concentrations were 400 mM $HClO_4$ or 86 mM $NaHCO_3/Na_2SiF_6$, leading to final concentrations of 20 mM $HClO_4$ or 4.3 mM $NaHCO_3/Na_2SiF_6$ in the samples analyzed, respectively. The IrO_2 NP stock concentration was 0.62 mM.

Sample	Vol. "acidity regulator" / mL	Vol. IrO_2 NP / mL	Vol. water / mL	Vol. ACN / mL	$[IrO_2$ NP] / μM
(i)	0.400	0	0.400	1.2	0
(ii)	0.400	0.080	0.320	1.2	6.2
(iii)	0.400	0.160	0.240	1.2	12.4
(iv)	0.400	0.240	0.160	1.2	18.6
(v)	0.400	0.320	0.080	1.2	24.8
(vi)	0.400	0.400	0	1.2	31.0

S5.4: Characterization of the reaction products in the presence of 10 % (v/v) water by ^{1}H NMR spectroscopy

^{1}H NMR spectroscopy was used to characterize the products of $[Ru(bpy)_3]^{3+}$ reduction both in the absence (Figure S12) and presence (Figure S13) of catalyst for the $NaHCO_3/Na_2SiF_6$ buffered system, as described in the Experimental section the main text. As seen in Figures S12 and S13, the clean pattern in the aromatic region clearly suggests the absence of degradation products. Decomposition of $[Ru(bpy)_3]^{3+}$ would manifest itself as the presence of a complex pattern as reported by Ghosh et al.[9]
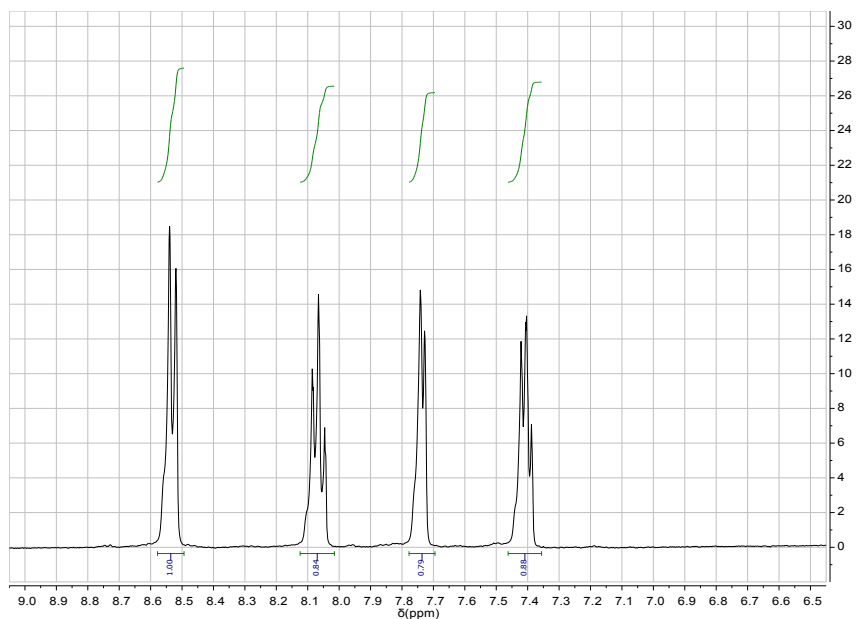
Figure S12. ^{1}H NMR spectrum for a sample of Ru(bpy)$_3$(bpy)$_3$(PF$_6$)$_3$ recorded after 30 minutes of reaction in the absence of catalyst. ACN-D3 was used as the solvent for Ru(bpy)$_3$(PF$_6$)$_3$. However, otherwise the experimental conditions were identical to those described in Figure 2B in the main text, *i.e.,* the sample contained 2 mM Ru(bpy)$_3$(PF$_6$)$_3$, and 4.3 mM NaHCO$_3$/Na$_2$SiF$_6$ buffer in a water/ACN-D3 mixture containing 25 % (v/v) of water.
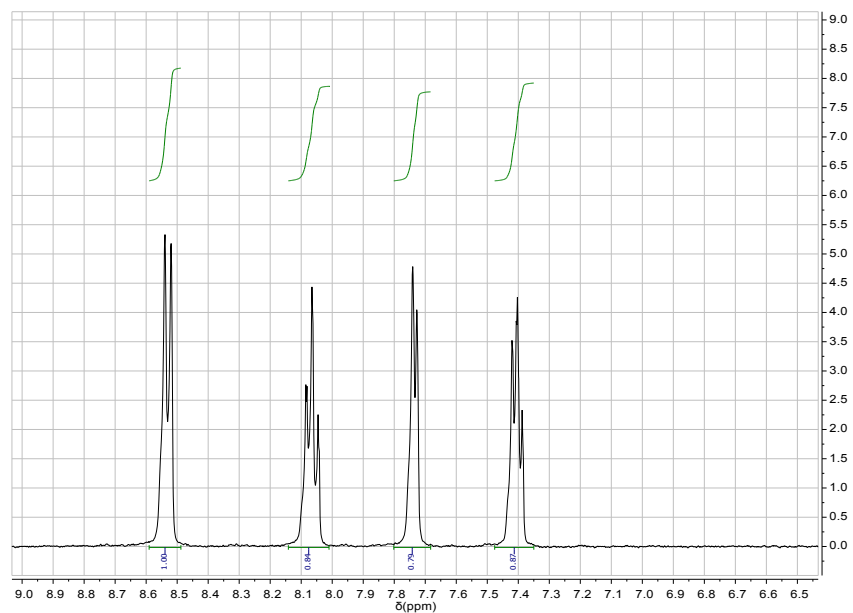
Figure S13. ^{1}H NMR spectrum for a sample of Ru(bpy)$_3$(bpy)$_3$(PF$_6$)$_3$ recorded after 30 minutes of reaction in the presence of catalyst. ACN-D3 was used as the solvent for Ru(bpy)$_3$(PF$_6$)$_3$. However, otherwise the experimental conditions were identical to those described in Figure 2B in the main text, *i.e.,* the sample contained 2 mM Ru(bpy)$_3$(PF$_6$)$_3$, 31 μM IrO$_2$ NPs and 4.3 mM NaHCO$_3$/Na$_2$SiF$_6$ buffer in a water/ACN-D3 mixture containing 25 % (v/v) of water.

S6: Influence of the water content on the kinetics of the WOR in a non-aqueous environment

S6.1: Infra-red (IR) spectroscopy of the water/ACN mixtures

The IR spectroscopy study by Takamuku *et al.* (ref. 48 in the main text) involved probing water/ACN mixtures containing 20 % D_2O at various water mole fractions (X_{H2O}). The premise of their study was to monitor wavenumber shifts as a function of X_{H2O} in water/ACN mixtures of (i) the O-D stretching mode of HDO, reflecting the extent of the formation of the water-water hydrogen bond network, and (ii) the C≡N stretching mode, reflecting the extent of the formation of hydrogen bonds between ACN and water molecules. Herein, this study is repeated using Takamuku *et al.*'s experimental conditions but incorporating the diverse additional species used during kinetic experiments monitoring the WOR in water/ACN mixtures, namely, sensitizer molecules ($Ru(bpy)_3(PF_6)_2$), acid ($HClO_4$) and heterogeneous catalytic species (IrO_2 NPs), as outlined in Figure 3 of the main article. The purpose of these control experiments is to eliminate the possibility that these augmented experimental conditions may invalidate our comparative analysis presented in the main text, between the kinetic data in Figure 3 and the data obtained by Takamuku *et al.*, in an unforeseen manner.

IR spectroscopic data was obtained over the wavenumber range 2200-3000 cm^{-1} for water/ACN mixtures containing all of the additional species noted *vide supra* and as a function of increasing X_{H2O}, with water containing 20 % D_2O (Figure S14). The chosen values of X_{H2O} directly compare with those reported by Takamuku *et al.* to facilitate ease of comparison between the two data sets. Three bands appear in the studied region of the IR spectrum, the major one at 2500-2640 cm^{-1} is attributed to the O-D stretching mode, while the other two

sharper bands at 2257 and 2295 cm^{-1} arise from the C≡N stretching mode and a combination of both CH$_3$ bending and C-C stretching in ACN, respectively.[10]

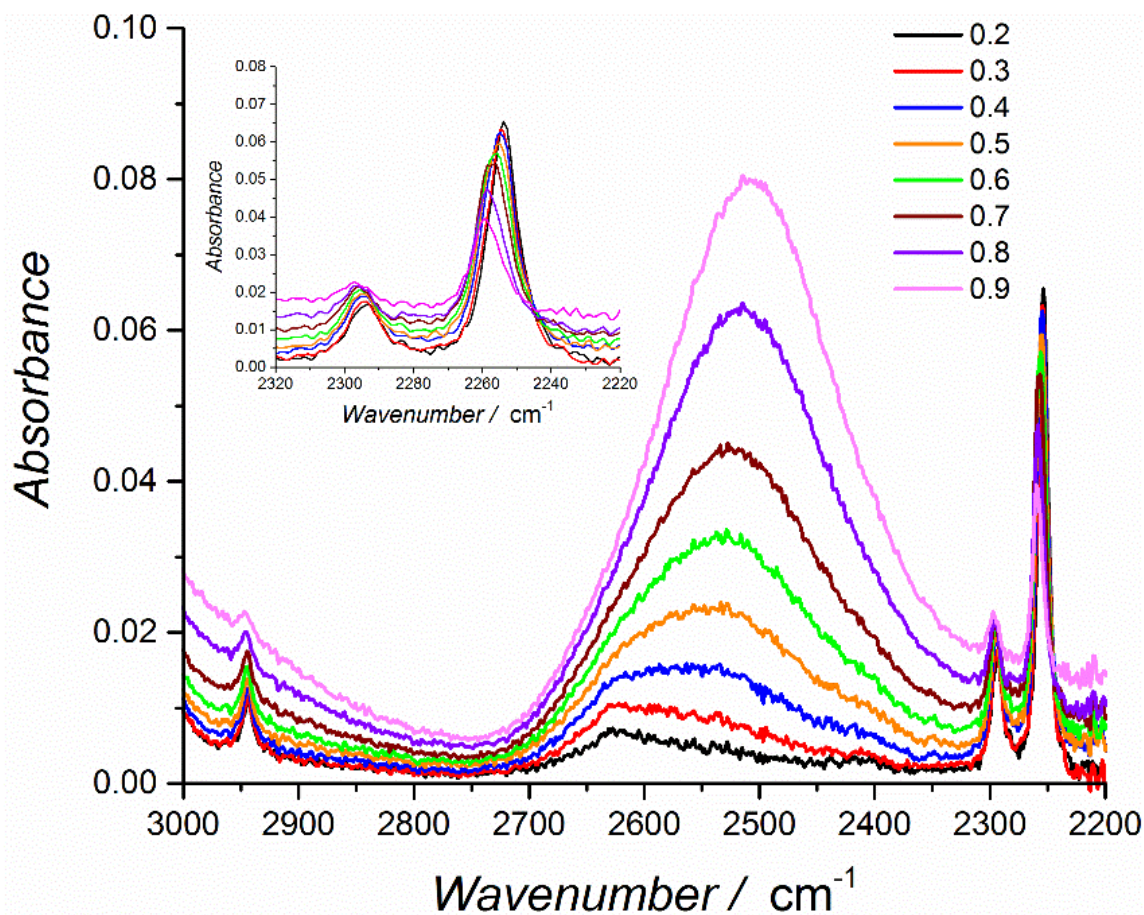**Figure S14.** Infra-red (IR) absorption spectra of water/ACN mixtures as a function of increasing water mole fraction (X_{H2O}) from X_{H2O} = 0.2 to 0.9.   The water contains 20 % D$_2$O. The concentrations of Ru(bpy)$_3$(PF$_6$)$_2$, HClO$_4$ and IrO$_2$ NPs in each ACN/water mixture were fixed at 2 mM, 20 mM and 27 µM, respectively.
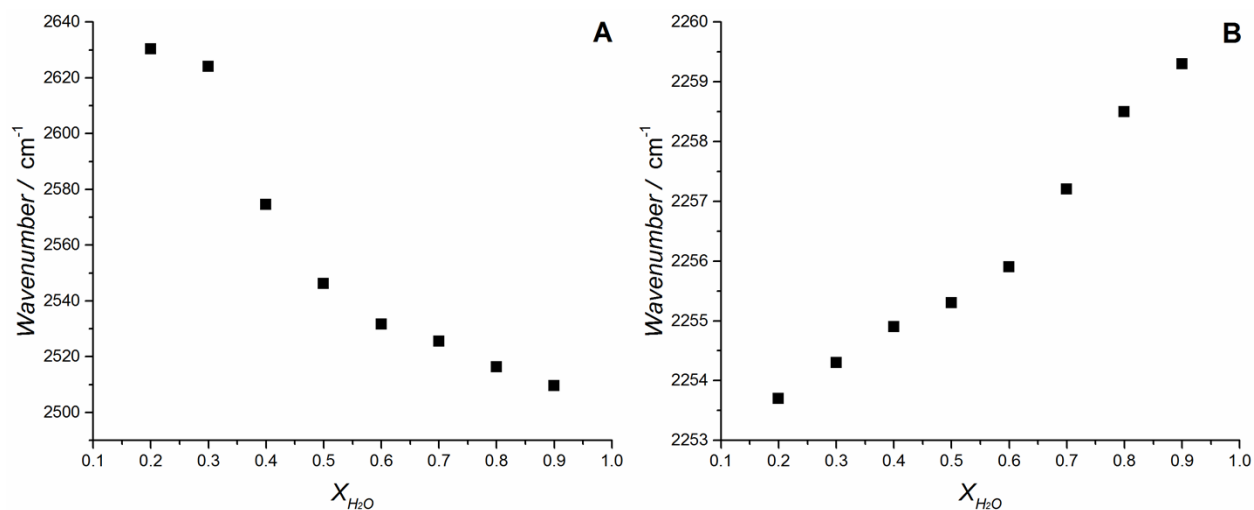
Figure S15. Wavenumbers for **(A)** the O-D stretching mode and **(B)** the C≡N stretching mode as a function of increasing water mole fraction (X_{H2O}) from X_{H2O} = 0.2 to 0.9. The water contains 20 % D_2O. The concentrations of Ru(bpy)$_3$(PF$_6$)$_2$, HClO$_4$ and IrO$_2$ NPs in each ACN/water mixture were fixed at 2 mM, 20 mM and 27 µM, respectively.

The wavenumbers of the O-D and C≡N stretching modes as a function of X_{H2O} were plotted in Figures S15 (A) and (B). The following broad trends were observed as X_{H2O} increases: (i) the wavenumber of the the O-D stretching mode decreases and (ii) the wavenumber of the C≡N stretching mode increases. The former trend is due to the progressive weakening of the O-D bond as the strength of the hydrogen-bonding network increases with increasing X_{H2O}. In particular, the wavenumber sharply decreases with increasing X_{H2O} from $X_{H2O} \approx 0.3$ to 0.6, directly in line with the trend seen by Takamuku *et al.* both from their IR spectroscopic and XRD analysis. The C≡N stretching mode may be de-convoluted into two Lorentzians, one at lower

wavenumbers assigned to free ACN molecules (as it only appears in pure ACN solvent) and one at slightly higher wavenumbers attributed to hydrogen-bonded ACN molecules (as it only appears in water/ACN mixtures). Whereas the wavenumbers of these Lorentzians do not vary significantly with increasing X_{H2O}, their relative intensities do change dramatically and produce an observed shift in the wavenumber of the C≡N stretching mode. Thus, as X_{H2O} increases from $X_{H2O} \approx 0.2$ to 0.9, the amount of hydrogen-bonded ACN molecules rapidly increases and the Lorentzian at higher wavenumbers increases in intensity. The latter is seen as an increase in wavenumber of the C≡N stretching mode, again directly in line with the trend seen by Takamuku *et al.* from their IR spectroscopic analysis.

Thus, the general conclusion from these control experiments is that we can replicate the trends observed by Takamuku *et al.* with the additional species present and that our comparative analysis in the main text is validated.

S6.2: Influence of the water content on the kinetics of $[Ru^{III}(bpy)_3]^{3+}$ reduction.

Herein, we describe in detail how each sample of varying water content, expressed in terms of percentage volume/volume (% (v/v)), in the presence of a $HClO_4$ "acidity regulator" at a constant $[IrO_2$ NP] was prepared for kinetics analysis. Three distinct regimes were identified with water contents (*i*) between 5 and 25 % (v/v), (*ii*) between 35 and 50 % (v/v), and (*iii*) between 70 and 85 % (v/v). Each regime required a slightly modified experimental approach when preparing the samples for kinetics analysis.

(*i*) **Water content between 5 and 25 % (v/v).** These experiments were carried out in an analogous fashion to those described in section S.5.2 by modifying the proportion of the mixture containing the catalyst, as shown in the table S4.

Table S4. Summary of the mixtures containing IrO_2 NPs, water and ACN used in the experiments to study the influence of the water content in the range 5 to 25 % (v/v). The IrO_2 NP stock concentration was 0.62 mM. The final concentrations of $HClO_4$ and IrO_2 NPs in the samples to be analyzed were 20 mM and 27 μM, respectively. *In this experiment the concentration of the acid solution was 3.2 M

Sample	Vol. 1 M $HClO_4$ / mL	Vol. water / mL	Vol. IrO_2 NPs / mL	Vol ACN / mL	Water content /% (v/v)
(*i*)	0.050*	0	0.350	1.6	5%
(*ii*)	0.160	0.290	0.350	1.2	10%
(*iii*)	0.160	0.690	0.350	0.8	15%
(*iv*)	0.160	1.49	0.350	0	25%

(ii) Water content between 35 and 50 % (v/v). For these experiments, 1.0 mL of 4 mM $Ru^{II}(bpy)_3(PF_6)_3$ solution was placed in a quartz cell. Subsequently, 1.0 mL of a solution containing water, ACN, $HClO_4$ and IrO_2 NPs was added and the absorbance at 673 nm and 900 nm recorded as a function of time. The mixtures were prepared as shown in the table S5.

Table S5. Summary of the mixtures containing IrO_2 NPs, water and ACN used in the experiments to study the influence of the water content in the range 35 to 50 % (v/v). The IrO_2 NP stock concentration was 0.62 mM. The final concentrations of $HClO_4$ and IrO_2 NPs in the samples to be analyzed were 20 mM and 27 μM, respectively

Sample	Vol. 0.5 M HClO$_4$ / mL	Vol. water / mL	Vol. IrO$_2$ NPs / mL	Vol ACN / mL	Water content /% (v/v)
(v)	0.160	1.065	0.175	0.6	35%
(vi)	0.160	1.665	0.175	0	50%

(iii) Water content between 70 and 85 % (v/v). For these experiments, a solution 2.67 mM Ru^{II}(bpy)$_3$(PF$_6$)$_3$ was dissolved in 26.67 mM HClO$_4$ prepared in water/ACN(13:2 (v/v)). As [Ru^{III}(bpy)$_3$]$^{3+}$ was found to be stable in acidic water-rich mixtures of water/ACN in the range of minutes, each solution was prepared immediately prior to analysis. 1.5 mL of the latter solution was placed in a quartz cell. Next, 0.5 mL of a solution containing water, ACN, and IrO$_2$ NPs was added and the absorbance at 673 nm and 900 nm recorded as a function of time. These mixtures were prepared as shown in the table S6.

Table S6. Summary of the mixtures containing IrO_2 NPs, water and ACN used in the experiments to study the influence of the water content in the range 70 to 85 % (v/v). The IrO_2 NP stock concentration was 0.62 mM. The final concentrations of $HClO_4$ and IrO_2 NPs in the samples to be analyzed were 20 mM and 27 μM, respectively

Sample	Vol. 0.5 M $HClO_4$ / mL	Vol. water / mL	Vol. IrO_2 NPs / mL	Vol ACN / mL	Water content /% (v/v)
(*vii*)	0.160	0.050	0.350	1.6	70%
(*viii*)	0.160	0.850	0.350	0.8	80%
(*ix*)	0.160	1.250	0.350	00.4	85%

S7: Continuous electrocatalytic O_2 evolution in water/ACN mixtures with $[Ru^{II}(bpy)_3]^{2+}$ as a redox shuttle

S7.1: Cyclic voltammetry of the $[Ru^{II}(bpy)_3]^{2+}$ redox shuttle in water /ACN mixtures using reticulated glassy carbon as the electrode.
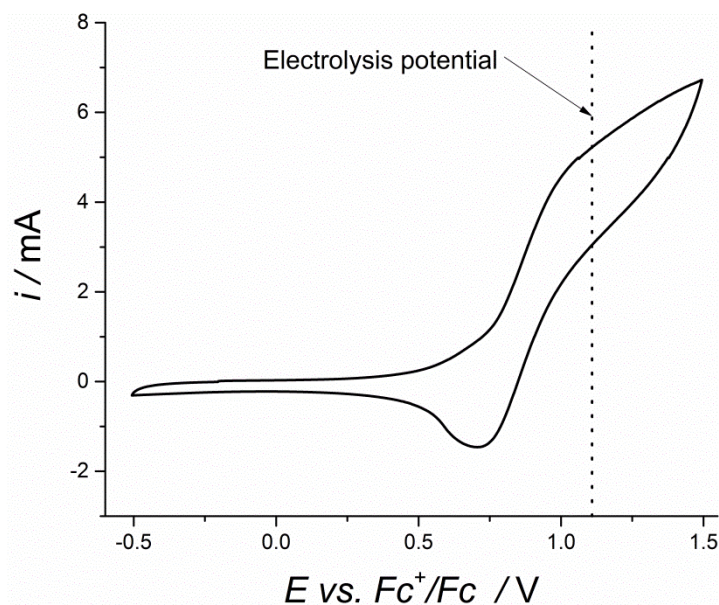

Figure S16. CV of a solution containing 2 mM Ru(bpy)$_3$(PF$_6$)$_2$, 31 µM IrO$_2$ NPs and 4.3 mM NaHCO$_3$/Na$_2$SiF$_6$ buffer in a water/ACN mixture (2.5:7.5 (v/v)).

S7.2: Bulk electrolysis control experiments: the influence of direct water oxidation in the absence of the $[Ru^{III}(bpy)_3]^{3+}/[Ru^{II}(bpy)_3]^{2+}$ redox couple and catalytic IrO$_2$ NPs.

During bulk electrolysis a potential is applied at the electrode surface that is sufficient to regenerate the $[Ru^{II}(bpy)_3]^{2+}$ redox shuttle but, in theory, not positive enough to overcome the overpotential for direct water oxidation during bulk electrolysis. As discussed in the main text of

the article, the latter potential was set 400 mV more positive than the cathodic peak of the [Ru^{III}]/[Ru^{II}] redox shuttle. A control experiment was thus performed to ensure that the extent of direct water oxidation at the electrode surface in the absence of both the [Ru^{III}]/[Ru^{II}] redox shuttle and catalytic IrO$_2$ NPs is minimal.

A comparative analysis of the currents and charge plots generated during bulk electrolysis of water/ACN mixtures (2.5/7.5 (v/v)) both the in the presence and absence of Ru(bpy)$_3$(PF$_6$)$_2$ and IrO$_2$ NPs is shown in Figure S17. The minimal contribution of direct water oxidation at the electrode surface is clearly highlighted by the relatively low charge passed after 1100 s of bulk electrolysis in the absence ($\approx$ 0.5 C) compared to the presence ($\approx$ 4.3 C) of both the [Ru^{III}]/[Ru^{II}] redox shuttle and catalytic IrO$_2$ NPs. Thus, under the precise experimental conditions described in Figure S17, the contribution of direct water oxidation at the electrode surface electrode is $\approx$11%.
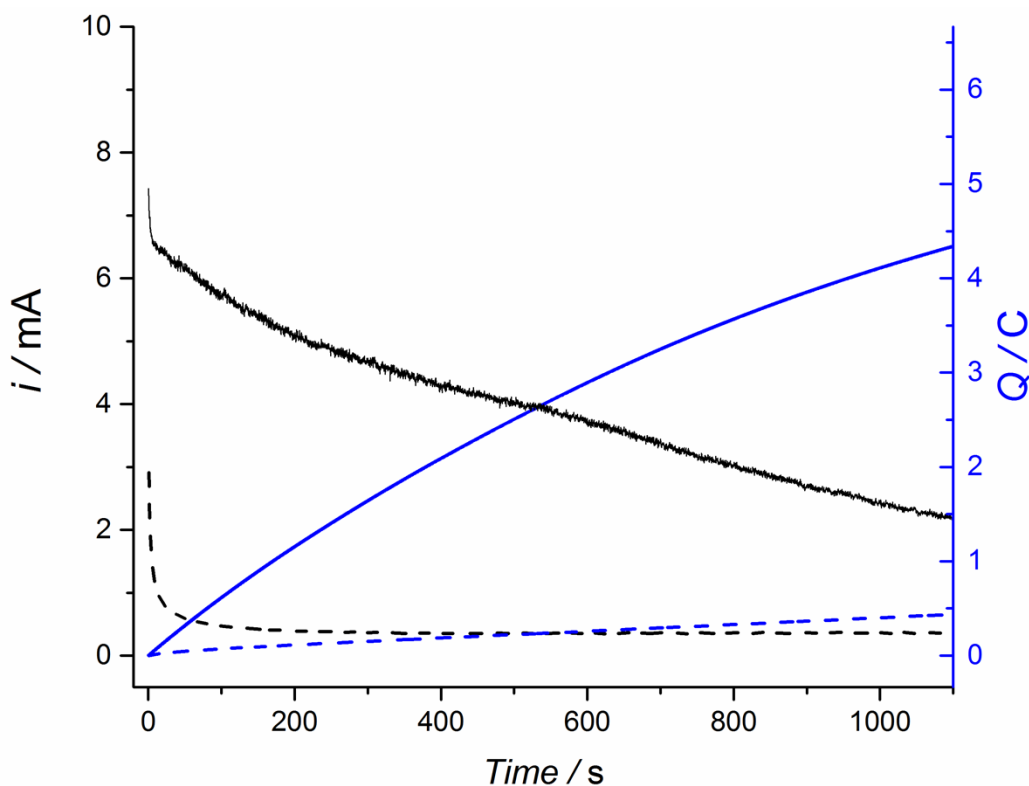
Figure S17. Control experiment: monitoring the extent of direct water oxidation at the electrode surface. The currents (black lines) and charge (blue lines) passed during bulk electrolysis of a solution containing 2 mM $Ru(bpy)_3(PF_6)_2$, 31 μM IrO_2 NPs and 4.3 mM $NaHCO_3/Na_2SiF_6$ buffer in a water/ACN mixture (2.5:7.5 (v/v)) are plotted and compared with the currents (dashed black line) and charge (dashed blue line) passed during bulk electrolysis in the absence of $Ru(bpy)_3(PF_6)_2$ and IrO_2 NPs, under otherwise identical experimental conditions.

S7.3: Monitoring the changes in viscosity of water/ACN mixtures with varying water content.

The analysis of the chronoamperometric curves obtained during bulk electrolysis at different water contents is rather complex due mainly to changes in the hydrodynamic conditions of the system. As the water content increases, the viscosity of the media as well as the diffusion coefficients of the electrotype species are modified. Thus, an analysis of the water content on the kinetics of the WOR based on the electrochemical response alone would be misleading. Figure S18 shows the variation of the viscosity of the water/ACN mixtures as a function of water content.
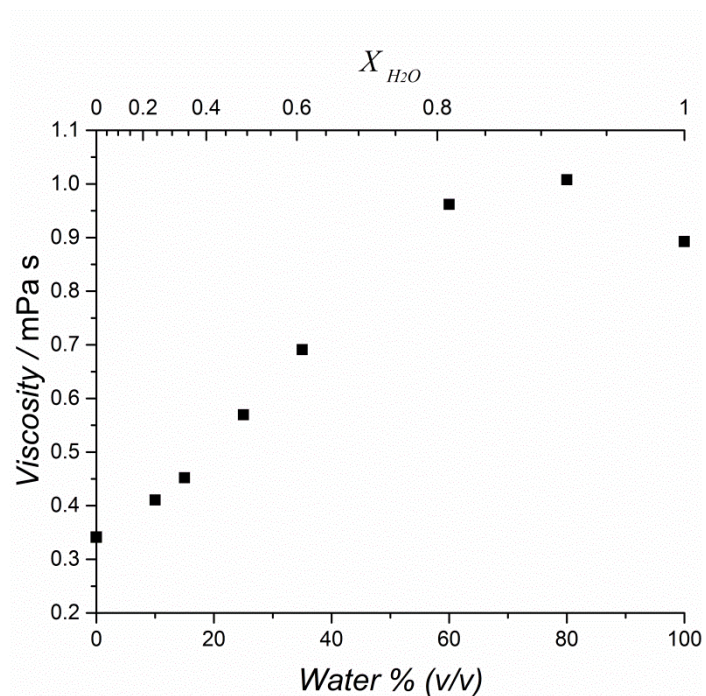
Figure S18. Viscosity of water/ACN mixtures at 25°C as a function of varying water content.

S8: Supplementary References

1. I. P. Evans, A. Spencer and G. Wilkinson, *J. Chem. Soc., Dalton Trans.*, 1973, 204.

2. Z. Ji, S. D. Huang and A. R. Guadalupe, *Inorg. Chim. Acta*, 2000, **305**, 127.

3. M. Biner, H. B. Buergi, A. Ludi and C. Roehr, *J. Am. Chem. Soc.*, 1992, **114**, 5197.

4. R. E. DeSimone and R. S. Drago, *J. Am. Chem. Soc.*, 1970, **92**, 2343.

5. M. Hara, C. C. Waraksa, J. T. Lean, B. A. Lewis and T. E. Mallouk, *J. Phys. Chem. A*, 2000, **104**, 5275.

6. N. D. Morris and T. E. Mallouk, *J. Am. Chem. Soc.*, 2002, **124**, 11114.

7. C. Franco and J. Olmsted Iii, *Talanta*, 1990, **37**, 905.

8. P. G. Hoertz, Y.-I. Kim, W. J. Youngblood and T. E. Mallouk, *J, Phys. Chem. B*, 2007, **111**, 6845.7

9. P. K. Ghosh, B. S. Brunschwig, M. Chou, C. Creutz and N. Sutin, *J. Am. Chem. Soc.*, 1984, **106**, 4772.

10. D. Jamroz, J. Stangret and J. Lindgren, *J. Am. Chem. Soc.*, 1993, **115**, 6165-6168.